Journal of Quantitative Spectroscopy & Radiative Transfer 250 (2020) 107037

Contents lists available at ScienceDirect

Journal of Quantitative Spectroscopy & Radiative Transfer

journal homepage: www.elsevier.com/locate/jqsrt

# Analysis of the hyperfine structure of the $Cs_2$ $3^3\Sigma_g^+$ state

Sofiia S. Onishchenko[a,b], Vladimir B. Sovkov[a,b,*], Feng Xie[c,*], Dan Li[d], Sergey S. Lukashov[b], Vera V. Baturo[b], Jizhou Wu[a,e], Jie Ma[a,e,f], Li Li[g]

[a] State Key Laboratory of Quantum Optics and Quantum Optics Devices, Institute of Laser spectroscopy, College of Physics and Electronics, Shanxi University, Taiyuan 030006, China
[b] St. Petersburg State University, 7/9 Universitetskaya nab., St. Petersburg 199034, Russia
[c] Institute of Nuclear and New Energy Technology, Collaborative Innovation Center of Advanced Nuclear Energy Technology, Key Laboratory of Advanced Reactor Engineering and Safety of Ministry of Education, Tsinghua University, Beijing 100084, China
[d] Center for Photonics and Electronics, Department of Precision Instruments, Tsinghua University, Beijing 100084, China
[e] Collaborative Innovation Center of Extreme Optics, Shanxi University, Taiyuan, Shanxi 030006, China
[f] College of Physics and Electronic Engineering, Shanxi University, 92 Wucheng Road, Taiyuan 030006, China
[g] Department of Physics, Tsinghua University, Beijing 100084, China

ARTICLE INFO

*Article history:*
Received 31 January 2020
Revised 15 April 2020
Accepted 15 April 2020
Available online 22 April 2020

*Keywords:*
Alkali metal dimers
Cesium molecule
Hyperfine structure
PFIIDR

ABSTRACT

We report on theoretical calculations and analyses of the hyperfine structures in the spectra of the $Cs_2$ $3^3\Sigma_g^+$ state observed by Li *et al* by infrared-infrared (IR-IR) double resonance spectroscopy in 2008. For this purpose, we consider the excitation–de-excitation schemes in their entirety, taking into account the mixed character of the intermediate levels of the $A^1\Sigma_u^+ \sim b^3\Pi_{\Omega u}$ system, which generally contains contributions from all $\Omega = 0,\ 1,\ 2$ basis states. We also avoid an approximation for the strongest features in the spectra (the major component), in which the probabilities of optical dipole transitions are computed from 0-th order state vectors alone. We compute the contributions from all components of the mixed states. The fundamental theory and algorithms are described, the parameters of the chosen model are fitted and reported, and the results of the simulation are presented.



## 1. Introduction

In last decades, alkali metal dimers are in the focus of experimental and theoretical research, because they open prospects for development of ultracold molecular trapping techniques [1–3], optimal control studies [4–7], quantum computing [6–15], and experimental investigation of few- and many-body quantum effects [16]. The subject of the present work is $Cs_2$, the heaviest stable alkali dimer, which was proposed as a reference system to check for a possible variation of the fundamental constants [17–20]. We already addressed some aspects of the $Cs_2$ spectroscopy in various electronic states in our earlier publications [21–30].

Alkali dimers exhibit a rich hyperfine structure (HFS) because they have two nuclei with non-zero spin. Information on the HFS [31–45] is essential to produce dimers in specific quantum states via photoassociation of the atomic pairs (see [6,27,46–54] and references within) or by tuning through zero-energy Feshbach resonances with magnetic fields (including the population of molecules' absolute ground states and the formation of Bose-Einstein or Fermi-Dirac condensates) [30].

In [55], Li et al. recorded the excitation spectra of the $Cs_2$ $3^3\Sigma_g^+$ state (dissociation limit $6S_{1/2} + 7S_{1/2}$) using the perturbation facilitated infrared-infrared double resonance (PFIIDR) experimental technique. They observed a rich rovibrational structure and constructed the potential energy function in the form of the Rydberg-Klein-Rees (RKR) curve and the expanded Morse oscillator. They also reported on partly resolved hyperfine structures (HFS), whose principal mechanism was attributed to the Fermi contact interaction, for many rovibrational levels. However, these HFS spectra have not been thoroughly analyzed or modeled since that work was published.

In recent years, we improved our computational algorithms and approaches so we were able to perform the analysis of the HFS in ultracold photoassociation spectra of the heteronuclear NaCs molecule [48,50,56]. Very recently, similar approaches have also been applied to the HFS in the perturbation facilitated optical-optical double resonance (PFOODR) spectra [57] of the $1^3\Delta_g$ state of the "hot" homonuclear molecule $Na_2$. These approaches consider most of the mechanisms neglected in earlier models [32,34], primarily the complete excitation–de-excitation schemes of the ex-

* Corresponding authors.
*E-mail addresses:* v.sovkov@spbu.ru, vladimir_sovkov@mail.ru (V.B. Sovkov), fxie@mail.tsinghua.edu.cn (F. Xie).

https://doi.org/10.1016/j.jqsrt.2020.107037
0022-4073/

periment and the mixed character of the window $A^1\Sigma_u^+ \sim b^3\Pi_{\Omega u}$ levels (see Secs. 3, 4 below).

The aims of this study include the adaptation of the aforementioned method to the case of the $Cs_2$ $3^3\Sigma_g^+$ state, modeling of all observed [55] HFS spectra, and determination of the fine and hyperfine interaction parameters. Totally, we have analyzed 52 such spectra, most of which had not been published yet.

## 2. Experimental details

Based on the widely used PFOODR technique [58–69], the PFIIDR was developed in studying the excited states of $K_2$, $Rb_2$, and $Cs_2$ [21–25,34,55,70–82]. So far, several excited states of $Cs_2$, including $3^3\Sigma_g^+$, $3^3\Pi_g$, etc., have been observed by this technique [21–24,55,78]. The experimental setup [55] is similar to that used in the $K_2$ PFIIDR experiments [70]. Briefly, two-step two-color excitation of the $Cs_2$ $3^3\Sigma_g^+$ state via mixed $A^1\Sigma_u^+ \sim b^3\Pi_{\Omega u}$ state have been realized. Cesium vapor was obtained by heating the Cs metal to approximately 300°C in the heatpipe with argon at the pressure of approximately 1 Torr used as a buffer gas. Two counter-propagating laser beams produced by single mode tunable Toptica DL 100 diode lasers with approximately 5 MHz linewidth (pump laser, 9620–9830 $cm^{-1}$ scanning range, ~25 mW power, and probe laser, 9560–9750 $cm^{-1}$ scanning range, ~30 mW power) overlapped at the center of a heatpipe. When the mixed intermediate state was excited from the ground state $X^1\Sigma_g^+$ by the pump laser, the upper state $3^3\Sigma_g^+$ can be detected by scanning the probe laser frequency and monitoring the $3^3\Sigma_g^+ \to a^3\Sigma_u^+$ fluorescence with a photomultiplier tube. Fixing the pump and probe lasers to excite a selected $3^3\Sigma_g^+$ level, we were able to measure $3^3\Sigma_g^+ \to a^3\Sigma_u^+$ fluorescence with a 0.85 m double grating Spex 1404 monochromator. The hyperfine structure of $3^3\Sigma_g^+$ can be investigated by the excitation spectroscopy, which was analyzed in detail in the current paper.

## 3. Theoretical model

Here, we present the Hamiltonian terms and their matrix elements that were actually used in our computations: a more complete model can be found in our previous works [48,50,57], although the present version is slightly altered. Notice, that the Hamiltonian terms and their matrix elements are given below in their full form targeted at dealing with any dimers and interactions. If the case of interactions within one multiplet and/or homonuclear diatomic molecule is considered, many of these equations can be reduced to simpler forms used in, e.g., [32,34,83–86]. The equations in the forms presented below are embedded in our computational codes. Throughout this section, the standard spectroscopic and group theory designations from [87] are used, analogous to [48,50,57]; terms related to the entire molecule and individual electrons are labeled with uppercase and lowercase letters, respectively.

### 3.1. Model Hamiltonian

The effective Hamiltonian for the system under study can be written as

$$\mathbf{H}^{(ef)} = (\mathbf{H}^{R} + \mathbf{H}^{CD}) + \mathbf{H}^{SS} + \mathbf{H}^{SR} + (\mathbf{H}^{FC} + \mathbf{H}^{DIP}). \quad (1)$$

The rotational part consists of the rotational term $\mathbf{H}^{R}$ and the centrifugal distortion term $\mathbf{H}^{CD}$:

$$\mathbf{H}^{R} = \left\langle v \left| \frac{\hbar^2}{2mr^2} \right| v \right\rangle \mathbf{R}^2 = B_v(\mathbf{J} - \mathbf{L} - \mathbf{S})^2 \quad (2)$$

$$\mathbf{H}^{CD} = -D_v(\mathbf{R}^2)^2. \quad (3)$$

We would like to emphasize that, even though the present work deals with fixed rotational states and concentrates on their hyperfine structure, the rotational terms are nevertheless essential and must be considered during the analysis. A blended state contains contributions from several $J$ and $\Omega$ components mixed by the mechanisms described below, which are influenced by the rotational parameters.

The spin–spin interaction (simplified form equivalent to previously used; see [32,34] and references therein) is

$$\mathbf{H}^{SS}_{simp} = \frac{2}{3}\lambda\left(3\mathbf{S}_z^2 - \mathbf{S}^2\right). \quad (4)$$

The spin-rotation interaction is as follows:

$$\mathbf{H}^{SR} = \gamma\mathbf{R}\cdot\mathbf{S} = \gamma\left[\mathbf{J}\cdot\mathbf{S} - \mathbf{L}\cdot\mathbf{S} - \mathbf{S}^2\right]. \quad (5)$$

The last two terms of Eq. (1) represent the hyperfine effects, namely, the Fermi contact interaction

$$\mathbf{H}^{FC} = \sum_{k=1}^{2}\sum_{i} b_F^{(ki)}\mathbf{I}_k\cdot\mathbf{s}_i \quad (6)$$

and the dipolar interaction (simplified form similar to previously used; see [32,34] and references therein)

$$\mathbf{H}^{DIP}_{simp} = \sum_{k=1}^{2}\frac{1}{3}c_d^{(k)}(3\mathbf{I}_{kz}\mathbf{S}_z - \mathbf{I}_k\cdot\mathbf{S}). \quad (7)$$

In (6) and (7) the summation runs over $k$ nuclei and $i$ valence electrons of the molecule.

In general, the Hamiltonian also includes terms corresponding to spin-orbit $\mathbf{H}^{SO}$ and electric quadrupole interaction $\mathbf{H}^{EQ}$, interaction between the spins of nuclei $\mathbf{H}^{II}$, between the molecular rotation and the nuclei spins $\mathbf{H}^{IR}$, and interaction between the electron orbits and the nuclei spins $\mathbf{H}^{IL}$. However, it was found that for $Cs_2$ their contributions were insignificant in our simulations, so we do not present explicit expressions for them.

### 3.2. Interaction matrix elements in the Hund's case ($a_\beta$) basis

The molecular states of the $\Sigma$ symmetry belong to the Hund's case ($b$) coupling scheme. However, it is often emphasized [88] that the Hund's case ($a$) basis is advantageous in that it has the maximum number of good quantum numbers. Within an approximation of the isolated multiplet (adopted by us currently) by either the case ($b$) or ($a$) basis sets, the same space of the physical states is considered and the results are equivalent. All equations and computer programs used in our earlier works [48,50,57] employed the Hund's case ($a_\beta$) basis. We use the same approach here for the analysis of the $Cs_2$ $3^3\Sigma_g^+$ state.

The Hund's case ($a_\beta$) basis state vectors are:

$$|nv\Lambda S\Sigma J(\Omega = \Lambda + \Sigma)IFM_F\rangle = |n\Lambda\rangle|S\Sigma\rangle|(J\Omega I)FM_F\rangle|vJ\rangle \quad (8)$$

with

$$|(J\Omega I)FM_F\rangle = \sum_{M_J M_I}\left|J\Omega M_J\right\rangle|IM_I\rangle\left\langle J\,M_J, I\,M_I|F\,M_F\right\rangle, \quad (9)$$

$$|IM_I\rangle = \sum_{M_{I_1}M_{I_2}}|I_1M_{I_1}\rangle|I_2M_{I_2}\rangle\langle I_1M_{I_1}I_2M_{I_2}|IM_I\rangle, \quad (10)$$

$n$ designates all non-specified quantum numbers. With the aim of brevity, further on we often use the designation $\mathcal{N} = \{nv\Lambda S\Sigma J\Omega IFM_F\}$ for the entire set of the Hund's case ($a_\beta$) quantum numbers.

With this basis, the matrix elements of the Hamiltomian terms listed above are presented below. In the formulae that follows, we emphasize the possible dependence of the parameters on the vibrational quantum number $v$ by introducing it in either the Dirac

bra-ket notation for the state vectors or as an extra subscript but omit their dependence on $J$, which is usually weaker due to a relatively weak dependence of the ro-vibrational wavefunctions on $J$. In the actual computations of the transition probabilities (22), the $J$ dependence of the wavefunctions in Eq. (23) was included (see the following section).

The rotational term $\mathbf{H}^{\mathrm{R}}$ (Eq. (2)) produces for its diagonal matrix element the case (a) rotational energy:

$$T_{vJ} = B_v\big[J(J+1) - \Omega^2 + S(S+1) - \Sigma^2\big] \tag{11}$$

and the $S$-uncoupling term for the only off-diagonal matrix element between the states with the same $\Lambda$ and $v$:

$$\big\langle \mathcal{N}|-B_v(\mathbf{J}_+\mathbf{S}_- + \mathbf{J}_-\mathbf{S}_+)|\mathcal{N}'\big\rangle = -B_v\delta_{\Lambda\Lambda'} \tag{12}$$

$$\times\delta_{II'}\delta_{FF'}\delta_{JJ'}\delta_{SS'}\Big\{\big[(J(J+1) - \Omega'(\Omega'-1))$$
$$\times\ (S(S+1) - \Sigma'(\Sigma'-1))\big]^{1/2}\delta_{\Omega,\Omega'-1}$$
$$+\big[(J(J+1) - \Omega'(\Omega'+1))$$
$$\times\ (S(S+1) - \Sigma'(\Sigma'+1))\big]^{1/2}\delta_{\Omega,\Omega'+1}\Big\}.$$

The matrix elements of the centrifugal distortion term $\mathbf{H}^{\mathrm{CD}}$ (Eq. (3)) can be found by a straightforward squaring the matrix of $\mathbf{H}^{\mathrm{R}}$:

$$\mathbf{H}^{\mathrm{CD}} = -D_v\big(\mathbf{H}^{\mathrm{R}}/B_v\big)^2. \tag{13}$$

The spin–rotation term $\mathbf{H}^{\mathrm{SR}}$ (Eq. (5)) produces the diagonal matrix element

$$\big\langle \mathcal{N}\big|\mathbf{H}^{\mathrm{SR}}\big|\mathcal{N}\big\rangle = \gamma_v\big(\Sigma^2 - S(S+1)\big). \tag{14}$$

The only off-diagonal element of $\mathbf{H}^{\mathrm{SR}}$ contributing to the case under consideration obtains the form (12) via the substitution $B_v \to -\frac{\gamma_v}{2}$.

The spin–spin interaction $\mathbf{H}^{\mathrm{SS}}_{\mathrm{simp}}$ in the simplified form of Eq. (4) only produces the diagonal matrix element:

$$\big\langle \mathcal{N}\big|\mathbf{H}^{\mathrm{SS}}_{\mathrm{simp}}\big|\mathcal{N}\big\rangle = \frac{2}{3}\lambda_v\big(3\Sigma^2 - S(S+1)\big). \tag{15}$$

The (presumably strongest) Fermi contact interaction $\mathbf{H}^{\mathrm{FC}}$ (Eq. (6)) and the dipolar interaction $\mathbf{H}^{\mathrm{DIP}}_{\mathrm{simp}}$ in the simplified form of Eq. (7) result in:

$$\big\langle \mathcal{N}\big|\mathbf{H}^{\mathrm{FC}}\big|\mathcal{N}'\big\rangle = \mathcal{C}\big(\{b_{\mathrm{F}k\nu}\}_{k=1}^2\big) \tag{16}$$

$$\times(-1)^{F-S+I+I'+I_1+I_2-\Lambda}\delta_{\Lambda\Lambda'}$$

and (with the extra condition $|\Sigma - \Sigma'| \le 1$)

$$\big\langle \mathcal{N}\big|\mathbf{H}^{\mathrm{DIP}}_{\mathrm{simp}}\big|\mathcal{N}'\big\rangle = \mathcal{C}\big(\{c_{\mathrm{d}k\nu}\}_{k=1}^2\big)(-1)^{F+I+I'+I_1+I_2+\Lambda-S+1}\delta_{\Lambda\Lambda'}\delta_{SS'}$$
$$\times\left[(\Sigma-\Sigma')^2 - \frac{2}{3}\right][(2S+1)S(S+1)]^{1/2} \tag{17}$$

respectively, where

$$\mathcal{C}\big(\{a_k\}_{k=1}^2\big) = \big[(2J+1)(2J'+1)(2I+1)(2I'+1)\big]^{1/2}$$
$$\times\begin{pmatrix} J & 1 & J' \\ \Omega & (\Omega'-\Omega) & -\Omega' \end{pmatrix}\begin{pmatrix} S & 1 & S \\ -\Sigma & (\Sigma-\Sigma') & \Sigma' \end{pmatrix}$$
$$\times\begin{Bmatrix} F & J' & I' \\ 1 & I & J \end{Bmatrix}\sum_{k=1}^{2}\left(\left[\begin{Bmatrix} I_1 & I & I_2 \\ I' & I_1 & 1 \end{Bmatrix}\delta_{k1}\right.\right.$$
$$\left.\left.+(-1)^{I-I'}\begin{Bmatrix} I_2 & I & I_1 \\ I' & I_2 & 1 \end{Bmatrix}\delta_{k2}\right]\right.$$
$$\left.\times\,[(2I_k+1)I_k(I_k+1)]^{1/2}a_k\right) \tag{18}$$

and the parameters are expressed as:

$$b_{\mathrm{F}k\nu} = \sum_i \big\langle n\nu\Lambda\big|b_{\mathrm{F}}^{(ki)}\big|n\nu\Lambda\big\rangle\big\langle S\big\|\tilde{\mathbf{T}}^1(\mathbf{s}_i)\big\|S'\big\rangle, \tag{19}$$

$$c_{\mathrm{d}k\nu} = \big\langle n\nu\Lambda\big|c_{\mathrm{d}}^{(k)}\big|n\nu\Lambda\big\rangle \tag{20}$$

with $\tilde{\mathbf{T}}^n(\mathbf{s})$ being the irreducible tensor operator of the $n$th rank of $\mathbf{s}$, the tilde symbol over it emphasizes that its components in the molecule-fixed coordinate system are of interest (this does not influence the resulting reduced matrix element and only deals with the ways of manipulating it).

In a case of a homonuclear molecule with $I_1 = I_2$, the coefficients at $a_1$ and $a_2$ in Eq. (18) are equal. Hence, separate contributions from $a_1$ and $a_2$ are indistinguishable, and an attempt to fit them separately would definitely result in a numerical instability. To avoid this setback, in our calculations we adopted effective parameters $\{a_1,\ a_2\} \to \{a_1(\mathrm{eff}) = a_2(\mathrm{eff}) = (a_1+a_2)/2\}$. In the basis of the properly symmetrized $g/u$-parity state functions, this happens automatically.

The relative probabilities (intensities) of electric dipole optical transitions with the electric vector $\boldsymbol{E}$ of an isotropic system:

$$B^{iso}_{nn'} = \frac{2\pi}{3\hbar^2}|\boldsymbol{E}|^2\big|\big\langle n\nu\ldots F\big\|\mathbf{T}^1(\boldsymbol{d})\big\|n'\nu'\ldots F'\big\rangle\big|^2 \tag{21}$$

can be computed using the reduced matrix element:

$$\big\langle \mathcal{N}\big\|\mathbf{T}^1(\boldsymbol{d})\big\|\mathcal{N}'\big\rangle = \delta_{SS'}\delta_{\Sigma\Sigma'}\delta_{II'}(-1)^{F'+I+\Omega+1} \tag{22}$$

$$\times\big[(2F+1)(2F'+1)(2J+1)(2J'+1)\big]^{1/2}$$

$$\times\begin{pmatrix} J' & 1 & J \\ -\Omega' & (\Omega'-\Omega) & \Omega \end{pmatrix}\begin{Bmatrix} J & F & I \\ F' & J' & 1 \end{Bmatrix}\mathcal{M},$$

with $\mathcal{M}$ being the matrix element of the dipole:

$$\mathcal{M} = \langle n\nu\Lambda|\tilde{\mathbf{T}}^1_{\Lambda-\Lambda'}(\boldsymbol{d})|n'\nu'\Lambda'\rangle. \tag{23}$$

## 4. Computational algorithm

In the experiment, the $3^3\Sigma_g^+ \to a^3\Sigma_u^+$ fluorescence was excited by PFIIDR

$$3^3\Sigma_g^+\ (v,\ N) \leftarrow A^1\Sigma_u^+ \sim b^3\Pi_u\ (J,\ k) \leftarrow X^1\Sigma_g^+\ (v_X,\ N_X) \tag{24}$$

We attempted to simulate the transitions at all stages.

In the works [55,89], the intermediate state $A^1\Sigma_u^+ \sim b^3\Pi_u$ levels were labeled by the rotational quantum number $J$ and the vibrational quantum number $v_A$ of the singlet component $A^1\Sigma_u^+$. However, it is recognized [90] that neither $v_A$ nor $v_b$ of the triplet component are good quantum numbers for the strongly mixed levels. In the present article, we use the numbering with $J,k$, where $k$ are the ordinal (in the ascending order of eigenenergies) numbers of the levels with the fixed $J$. This way of numbering follows the suit of [91].

The procedure of simulation was as follows. At first, we obtained the eigenenergies and eigenfunctions of the HF components for a single selected $3^3\Sigma_g^+$ vibrational state. To do that, we constructed and diagonalized the Hamiltonian matrix in the Hund's case ($a_\beta$) basis. As mentioned earlier, the $3^3\Sigma_g^+$ state is closer to the Hund's case ($b$), and its levels are characterized by the rotational quantum number $N$. So, we included all $J = N,\ N \pm 1$ state functions in the basis sets.

Then, we consistently analyzed all steps of the excitation–de-excitation scheme. Namely, we computed the probabilities of the optical transitions on the first step of excitation scheme to predict the populations of different $I,F$ components of the $A^1\Sigma_u^+ \sim b^3\Pi_u$ system in assumption that the excitation occurs from a single rovibrational level of the $X^1\Sigma_g^+$ ground state with equally populated

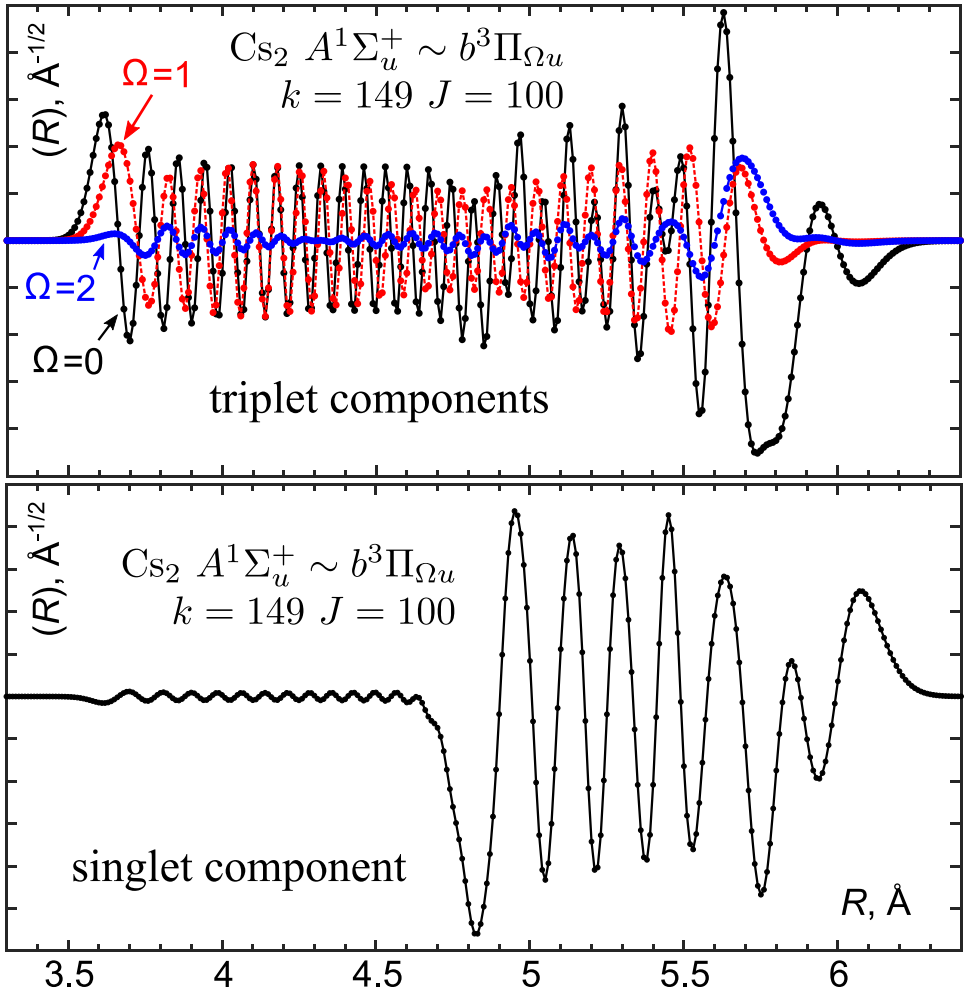


**Fig. 1.** The vibrational wavefunctions of the $Cs_2$ $A^1\Sigma_u^+ \sim b^3\Pi_u$ ($J = 100$, $k = 149$) triplet (upper panel) and singlet (lower panel) state components [91]. The dots of the computational grid are connected with the straight lines. For ease of comprehension, the amplitudes of the $\Omega = 1$ component are multiplied by a factor of 20, and those of the $\Omega = 2$ component are multiplied by a factor of 200.

non-blended $(I, F)$ sublevels. Further, we computed populations of the $3^3\Sigma_g^+$ state HF components as the probabilities of optical transitions on the second step of (24), taking into account calculated populations of $F, I$ components of $A^1\Sigma_u^+ \sim b^3\Pi_u$ mixed state.

A blended character of the $A^1\Sigma_u^+ \sim b^3\Pi_u$ intermediate levels was considered within the model presented in [91] taking into account the contributions from their different Ω components. When our analysis had been completed and the present paper had been finalizing, we found out that the new experimental data and the renewed analysis of the $Cs_2$ $A^1\Sigma_u^+ \sim b^3\Pi_u$ system were published in [92]. A switch to this newer model from the one of [91] used by us currently cannot influence our results substantially, as the older model [91] was already very reliable within the energy range of our interest. We intend to switch to the new model [92] in our future research of the $Cs_2$ spectroscopy.

It was found that the coupling of the different Ω components of the $Cs_2(A^1\Sigma_u^+ \sim b^3\Pi_u)$ system based on the model of [91] significantly altered the shapes of their vibrational (coordinate) wavefunctions, in contrast to the case of $Na_2$ discussed in [57,93]. Sample characteristic wavefunctions are given in Fig. 1. So, we were not able to use the individual Ω fraction amplitudes $\|\Psi_\Omega\|^\pm$ in the mixed intermediate states as signed (notice the "±" superscript) weights of their contributions to the optical transition probability amplitudes, in place of the matrix elements $\mathcal{M}$ in Eq. (22), as it was done in [57]. The algorithm utilized in the present paper was more complicated. Specifically, we computed the vibrational wavefunctions of all Ω components of the $A^1\Sigma_u^+ \sim b^3\Pi_u$ intermediate levels within the model of [91] and the vibrational wavefunctions of the levels of the upper $3^3\Sigma_g^+$ state based on the potential energy functions from [55]; then, we substituted their overlap integrals as factors $\mathcal{M}$ for the optical transition probability amplitudes in Eq. (22). For this purpose, we used our programs utilizing the coupled channel Fourier grid method [94–96].

Finally, we simulated the intensity distributions in the experimental HFS spectra as the probabilities of the optical transitions from these states, into an effective vibrational level of the $a^3\Sigma_u^+$ state with the $J'$ quantum number ranging from $N-2$ to $N+2$ taking into account precomputed $3^3\Sigma_g^+$ populations. The computed probabilities ("discrete spectra") were convolved with the Lorentzian functions, which approximate the line profiles. During the optimization, the widths of the Lorentzians were fitted along with the interaction parameters.

The computations were repeated iteratively with parameters of the fine and hyperfine interactions being varied until the best reproduction of the experimental spectra was achieved. We used the computer package "Optimizer" for this purpose, utilizing the Levenberg–Marquardt scheme of the least square fit based on the singular value decomposition (SVD) of the design matrix, which is

**Table 1**
List of the observed [55,89] and modeled HFS spectra $3^3\Sigma_g^+$ $(v,\ N,\ T) \leftarrow A^1\Sigma_u^+ \sim b^3\Pi_u$ $(J,\ k,\ T_k)$ with their vibrational $v$ and rotational $N$, $J$ quantum numbers and term values $T, T_k$ (relative to the bottom of the ground state, $cm^{-1}$); $k$ is the ordinal number from below of the mixed intermediate level [91] with the fixed $J$. All the term values $T_k$, $T$ are experimental [55,89,91].

| $J$ | $k$ | $T_k$ | $v$ | $N$ | $T$ | $J$ | $k$ | $T_k$ | $v$ | $N$ | $T$ |
|---|---|---|---|---|---|---|---|---|---|---|---|
| 70 | 124 | 9841.487 | 2 | 69 | 19577.290 | 100 | 149 | 10127.275 | 5 | 99 | 19705.761 |
| 70 | 124 | 9841.487 | 2 | 71 | 19579.761 | 100 | 149 | 10127.275 | 5 | 101 | 19709.236 |
| 24 | 138 | 9919.486 | 3 | 25 | 19569.028 | 101 | 149 | 10129.202 | 5 | 100 | 19707.472 |
| 42 | 134 | 9890.912 | 3 | 41 | 19578.422 | 101 | 149 | 10129.202 | 5 | 102 | 19710.983 |
| 42 | 134 | 9890.912 | 3 | 43 | 19579.911 | 102 | 149 | 10131.131 | 5 | 101 | 19709.235 |
| 44 | 134 | 9892.509 | 3 | 43 | 19579.911 | 102 | 149 | 10131.131 | 5 | 103 | 19712.779 |
| 44 | 134 | 9892.509 | 3 | 45 | 19581.469 | 160 | 142 | 10230.798 | 5 | 159 | 19839.310 |
| 46 | 133 | 9894.180 | 3 | 45 | 19581.469 | 99 | 149 | 10125.344 | 6 | 98 | 19731.807 |
| 46 | 133 | 9894.180 | 3 | 47 | 19583.097 | 100 | 149 | 10127.275 | 6 | 99 | 19733.533 |
| 24 | 138 | 9919.486 | 4 | 23 | 19596.476 | 101 | 149 | 10129.202 | 6 | 100 | 19735.238 |
| 24 | 138 | 9919.486 | 4 | 25 | 19597.331 | 101 | 149 | 10129.202 | 6 | 102 | 19738.735 |
| 42 | 134 | 9890.912 | 4 | 41 | 19606.694 | 102 | 149 | 10131.131 | 6 | 101 | 19736.995 |
| 42 | 134 | 9890.912 | 4 | 43 | 19608.178 | 100 | 149 | 10127.275 | 8 | 99 | 19788.686 |
| 44 | 134 | 9892.509 | 4 | 43 | 19608.177 | 100 | 149 | 10127.275 | 8 | 101 | 19792.129 |
| 44 | 134 | 9892.509 | 4 | 45 | 19609.731 | 102 | 149 | 10131.131 | 8 | 101 | 19792.128 |
| 46 | 133 | 9894.180 | 4 | 45 | 19609.730 | 102 | 149 | 10131.131 | 8 | 103 | 19795.637 |
| 46 | 133 | 9894.180 | 4 | 47 | 19611.353 | 160 | 142 | 10230.799 | 8 | 159 | 19920.927 |
| 78 | 141 | 10010.650 | 4 | 77 | 19644.027 | 170 | 151 | 10342.526 | 8 | 169 | 19948.718 |
| 78 | 141 | 10010.650 | 4 | 79 | 19646.759 | 172 | 151 | 10348.822 | 8 | 171 | 19954.471 |
| 160 | 142 | 10230.798 | 4 | 159 | 19811.860 | 102 | 149 | 10131.131 | 9 | 101 | 19819.493 |
| 222 | 137 | 10446.996 | 4 | 223 | 20019.921 | 102 | 149 | 10131.131 | 9 | 103 | 19823.001 |
| 224 | 137 | 10455.103 | 4 | 223 | 20019.921 | 172 | 151 | 10348.822 | 9 | 173 | 19987.101 |
| 226 | 137 | 10463.276 | 4 | 225 | 20027.468 | 100 | 149 | 10127.275 | 10 | 99 | 19843.339 |
| 78 | 141 | 10010.650 | 5 | 77 | 19672.043 | 100 | 149 | 10127.275 | 10 | 101 | 19846.760 |
| 78 | 141 | 10010.650 | 5 | 79 | 19674.764 | 172 | 151 | 10348.822 | 11 | 171 | 20034.653 |
| 99 | 149 | 10125.344 | 5 | 100 | 19707.471 | 172 | 151 | 10348.822 | 11 | 173 | 20040.331 |

described in [97] with the downloadable source codes available at [98].

We worked with a set of archived files containing the spectra at Tsinghua University, most of which had not been published anywhere else. The spectra were labeled as $3^3\Sigma_g^+$ $(v,\ N) \leftarrow A^1\Sigma_u^+$ $(v_A,\ J)$. Due to the mixed character of the state function, this labeling is not unambiguous and unable to uniquely characterize the intermediate window levels. The term values of the intermediate levels that were actually used in the experiments could be extracted from Tables A.1 and E of [89]; the model of [91] allowed us to determine the ordinal numbers $k$ of these levels. The spectra we have analyzed are listed in Table 1 with the unambiguous labeling and term values.

It can be seen from Table 1 that among 52 spectra analyzed in the present paper there are two spectra of rotational levels that belong to $v = 2$, seven that belong to $v = 3$, fourteen that belong to $v = 4$, ten that belong to $v = 5$, five that belong to $v = 6$, seven that belong to $v = 8$, three that belong to $v = 9$, two that belong to $v = 10$, and two that belong to $v = 11$. The total data set includes levels belonging to the range of rotational quantum numbers $N =$ 23–225 and vibrational quantum numbers $v = 2$–11.

We were unable to locate the characteristics of the initial ground $X^1\Sigma_g^+$ state levels in the schemes from Eq. (24). However, the vibrational quantum number $v_X$ plays no role in computing the relative intensities, and differences in the HFS spectra lineshapes for the schemes beginning with $N_X = J - 1$ and $N_X = J + 1$ are negligible.

The total parity of a state of $\Sigma^+$ symmetry is $(-1)^N$. For the homonuclear $Cs_2$ molecule, only even values $I = 0, 2, 4, 6$ of the total nuclear spin can exist in the positive parity rotational $3^3\Sigma_g^+$ states and only odd values $I = 1, 3, 5, 7$ can exist in the negative parity rotational $3^3\Sigma_g^+$ states. Therefore, it is expected that 9 major HF features will be produced from the $3^3\Sigma_g^+$ levels with odd rotational quantum numbers $N$, and 7 major HF features will be produced from the $3^3\Sigma_g^+$ levels with even rotational quantum numbers $N$. In most of the experimental HFS spectra, such features are recognizable.

## 5. Results and discussion

We fitted the observed spectra of each of the $3^3\Sigma_g^+$ $(v =$ 2, 3, 4, 5, 6, 8, 9, 10, 11) vibrational levels separately to the global models described in the previous sections. We used the numerical values of the rotational constants $B_v$ and the centrifugal distortion constants $D_v$ for all of these levels from [55]. All other parameters were optimized in the fit.

The following are examples of the final simulations of the $Cs_2$ $3^3\Sigma_g^+$ excitation spectra with the HFS [55]:

- $3^3\Sigma_g^+$ $(v = 2,\ N = 71) \leftarrow A^1\Sigma_u^+ \sim b^3\Pi_u$ $(J = 70,\ k = 124)$ transition is shown in Fig. 2.
- $3^3\Sigma_g^+$ $(v = 3,\ N = 43) \leftarrow A^1\Sigma_u^+ \sim b^3\Pi_u$ $(J = 44,\ k = 134)$ transition is shown in Fig. 3.
- $3^3\Sigma_g^+$ $(v = 4,\ N = 41) \leftarrow A^1\Sigma_u^+ \sim b^3\Pi_u$ $(J = 42,\ k = 134)$ transition is shown in Fig 4.
- $3^3\Sigma_g^+$ $(v = 6,\ N = 102) \leftarrow A^1\Sigma_u^+ \sim b^3\Pi_u$ $(J = 101,\ k = 149)$ transition is shown in Fig. 5.
- $3^3\Sigma_g^+$ $(v = 10,\ N = 101) \leftarrow A^1\Sigma_u^+ \sim b^3\Pi_u$ $(J = 100,\ k = 149)$ transition is shown in Fig. 6.

These spectra represent features specific to the HFS with negative $(v = 6)$ and positive $(v = 2,\ 3,\ 4,\ 10)$ parity. The final sets of parameters for all of the experimentally observed vibrational levels are listed in Table 2.

Summarizing, we have estimated all relevant parameters in our model for the HFS of the $Cs_2$ $3^3\Sigma_g^+$ state. The Fermi contact interaction (FC) is the dominant source of the hyperfine splitting. For each vibrational level, the FC has a separately determined value; however, the differences between these vibration–dependent parameters are not large (Table 2). Next in importance is the spin-rotation interaction (SR). The other two interactions have a smaller effect on the line shapes in the theoretical model but still affect the simulated feature-shapes. These are the spin–spin (SS) and nuclear dipolar (DIP) interactions.

According to [48], the asymptotic near–dissociation value of the molecular electronic spatial diagonal matrix element of the Fermi

**Table 2**
Parameters of the fine and hyperfine interactions estimated from a fit of the experimental HF spectra of the $Cs_2$ $3^3\Sigma_g^+$ state. All values are expressed in wavenumbers ($cm^{-1}$), estimated standard deviations (for the last decimal digits reported) in the parenthesis, the character "e" designates the decimal order.

| $v$ | $b_{F1v} = b_{F2v}$ (FC) | $\gamma$ (SR) | $\lambda$ (SS) | $c_{d1v} = c_{d2v}$ (DIP) |
|---|---|---|---|---|
| 2 | 4.5044(26)e−2 | 5.00(1)e−4 | 7.102(9)e−2 | 1.82(7)e − 3 |
| 3 | 5.186 89(5)e−2 | 7.84(2)e−5 | 6.4906(7)e−2 | 2.081(2)e−2 |
| 4 | 5.1699(7)e−2 | 6.59(2)e−5 | 6.6343(33)e−2 | 2.084 19(1 70)e−2 |
| 5 | 5.245 40(8)e−2 | 5.06(3)e−5 | 7.074(3)e−2 | 2.2219(19)e−2 |
| 6 | 5.2012(11)e−2 | 6.47(3)e−5 | 6.614(5)e−2 | 2.246 90(3)e−2 |
| 8 | 5.2734(10)e−2 | 6.55(2)e−5 | 6.701 594(15)e−2 | 2.5458(28)e−2 |
| 9 | 5.2125(19)e−2 | 6.63(5)e−5 | 6.351(2)e−2 | 2.294(5)e−2 |
| 10 | 5.3901(16)e−2 | 3.450(4)e−4 | 6.6900(5)e−2 | 1.454(4)e−2 |
| 11 | 4.93(3)e−2 | 3.853(3)e−4 | 7.573(8)e−2 | 1.439(7)e−2 |

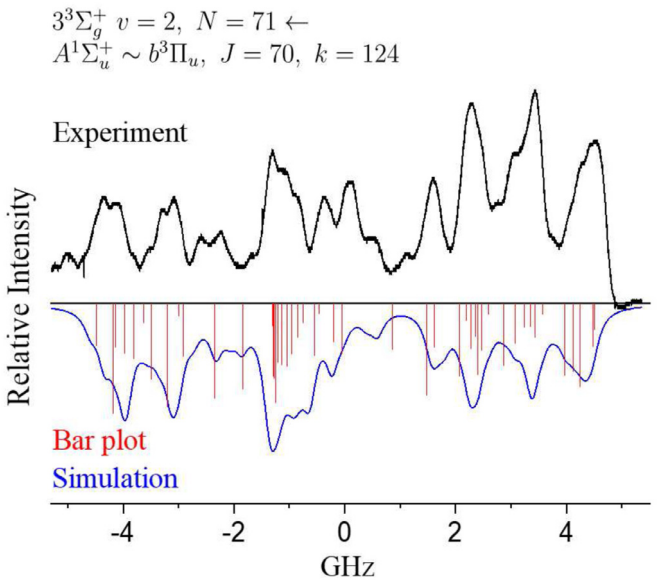


**Fig. 2.** HFS spectrum $Cs_2$ $3^3\Sigma_g^+$ ($v = 2$, $N = 71$) $\leftarrow A^1\Sigma_u^+ \sim b^3\Pi_u$ ($J = 70$, $k = 124$): experiment, simulation.

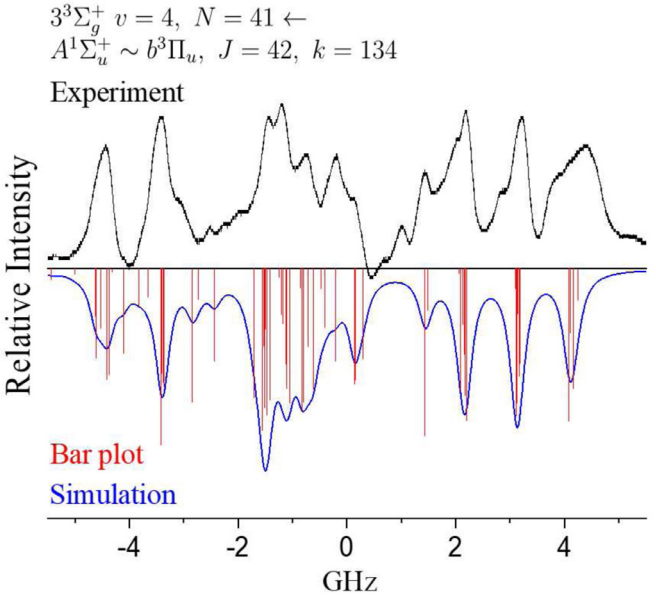


**Fig. 4.** HFS spectrum $Cs_2$ $3^3\Sigma_g^+$ ($v = 4$, $N = 41$) $\leftarrow A^1\Sigma_u^+ \sim b^3\Pi_u$ ($J = 42$, $k = 134$): experiment, simulation.

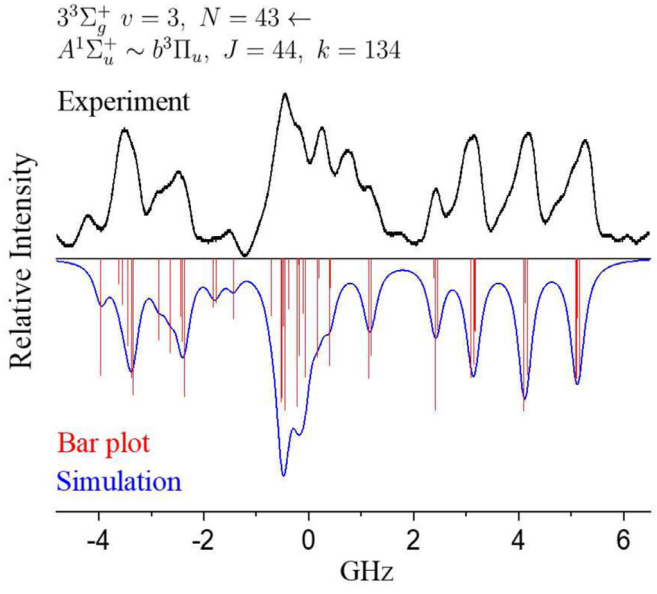


**Fig. 3.** HFS spectrum $Cs_2$ $3^3\Sigma_g^+$ ($v = 3$, $N = 43$) $\leftarrow A^1\Sigma_u^+ \sim b^3\Pi_u$ ($J = 44$, $k = 134$): experiment, simulation.

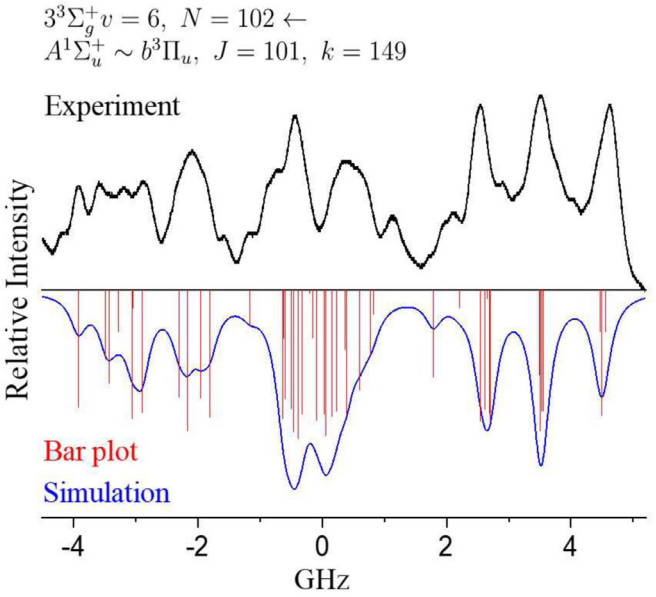


**Fig. 5.** HFS spectrum $Cs_2$ $3^3\Sigma_g^+$ ($v = 6$, $N = 102$) $\leftarrow A^1\Sigma_u^+ \sim b^3\Pi_u$ ($J = 101$, $k = 149$): experiment, simulation.

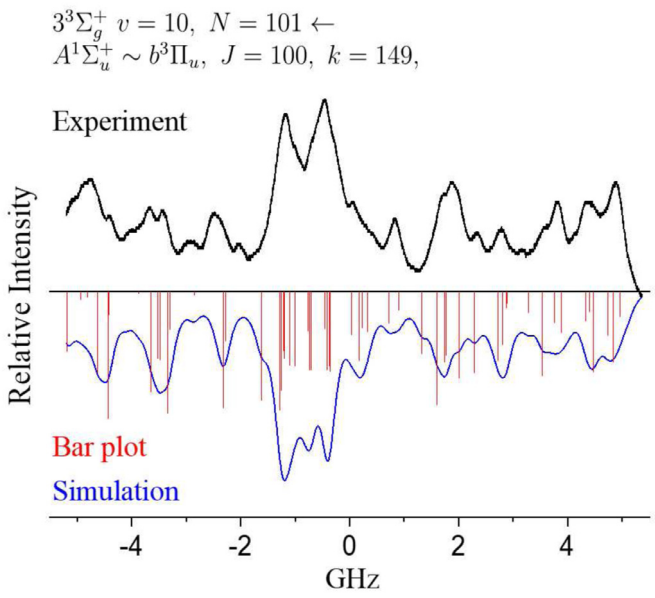


**Fig. 6.** HFS spectrum $Cs_2$ $3^3\Sigma_g^+$ ($v = 10$, $N = 101$) $\leftarrow A^1\Sigma_u^+ \sim b^3\Pi_u$ ($J = 100$, $k = 149$): experiment, simulation.

contact interaction is the half sum of the corresponding atomic parameters as they defined in [48]. The dominating such parameter in the Cs $6S_{1/2}$ state was estimated [48] to be $\sim 1.15$ GHz ($3.83\times 10^{-2}$ cm$^{-1}$). After the summation, the spin factor in Eq. (19) equals $\sqrt{6}$ resulting in the asymptotic estimate $b_{Fkv}^{\infty} = 4.69\times 10^{-2}$ cm$^{-1}$. The values in Table 2 are close to this estimate but somewhat larger due to a contribution from the Cs $7S_{1/2}$ atomic state ($\sim 1.0\times 10^{-2}$ cm$^{-1}$) as well as the exchange effect.

The current simulation reproduces satisfactorily the line shapes in the spectra. The remaining discrepancies can be of different origin. First, due to a high density of states in the observed energy range, there can be accidental optical resonances with other rovibronic levels, whose fluorescence overlaps the observed ones and distorts the line shapes. Second, in spite of the relatively high temperature and pressure of the buffer gas, presumably destroying the alignment of the molecules at every next step of the excitation scheme, there can be some residual alignment not taken into account in our present model. Third, the collisions, besides destroying the alignment, can also alter the relative populations of the hyperfine components in the intermediate and upper rovibronic states. Fourth, perturbations from some neighboring levels belonging to other electronic states cannot be excluded as well. Theoretically, the hyperfine splitting of the intermediate $A^1\Sigma_u^+ \sim b^3\Pi_u$ levels can also contribute to the observed spectra but we are unaware about an observation of such noticeable splitting—the model of [91,92] does not include hyperfine interactions and proved to be very reliable and accurate.

In order to estimate the role of those mechanisms and include them into the model, extra rather difficult experiments are needed, which are not available for us currently, as well as a substantial complication of the theoretical model and the computational algorithm. On the other hand, the present model is already a step forward from the aforementioned earlier models [32,34] and is able to reproduce the experimental HFS spectra reliably.

## 6. Conclusions

The algorithm and computational approaches for simulation and analysis of the hyperfine spectra in homonuclear diatomic molecules were applied to the case of the HFS spectra of the $Cs_2$ $3^3\Sigma_g^+$ state. The analysis was successfully conducted and, to the best of our knowledge, is the first such analysis to be conducted.

## Declaration of Competing Interest

The authors declare that they have no known competing financial interests or personal relationships that could have appeared to influence the work reported in this paper.

## CRediT authorship contribution statement

**Sofiia S. Onishchenko:** Investigation, Formal analysis, Writing - original draft. **Vladimir B. Sovkov:** Conceptualization, Methodology, Software, Writing - original draft. **Feng Xie:** Investigation, Writing - original draft. **Dan Li:** Investigation. **Sergey S. Lukashov:** Investigation, Writing - original draft. **Vera V. Baturo:** Investigation, Writing - original draft. **Jizhou Wu:** Investigation, Validation. **Jie Ma:** Investigation, Validation. **Li Li:** Methodology, Supervision.

## Acknowledgments

S. Onishchenko is grateful to the support from the exchanging program of Shanxi University. This work was supported by the National Key R&D Program of China (Grant No. 2017YFA0304900), NNSF of China (Grant Nos. 11604177, 11811530068, 11574177, 61722507 and 61675121), 111 project (Grant No.D18001), the Program for the Outstanding Innovative Teams of Higher Learning Institutions of Shanxi (OIT), and the collaborative grants by the Russian Foundation for Basic Research (RFBR) and NNSF of China (No. 18-53-53030 and No. 20-53-53025 in the RFBR classification).

## References

[1] Barry JF, McCarron DJ, Norrgard EB, Steinecker MH, DeMille D. Magneto-optical trapping of a diatomic molecule. Nature 2014;512:286–96. doi:10.1038/nature13634.
[2] Anderegg L, Augenbraun BL, Bao Y, Burchesky S, Cheuk LW, Ketterle W, et al. Laser cooling of optically trapped molecules. Nat Phys 2018;14(9):890–3. doi:10.1038/s41567-018-0191-z.
[3] Sautenkov VA, Saakyan SA, Bobrov AA, Kudrinskiy DA, Vilshanskaya EV, Zelener BB. Optical dipole trap for laser-cooled lithium-7 atoms. J Russ Laser Res 2019;40(3):230–6. doi:10.1007/s10946-019-09794-4.
[4] Jaouadi A, Barrez E, Justum Y, Desouter-Lecomte M. Quantum gates in hyperfine levels of ultracold alkali dimers by revisiting constrained–phase optimal control design. J Chem Phys 2013;139(1):014310. doi:10.1063/1.4812317.
[5] Lysebo M, Veseth L. Quantum optimal control theory applied to transitions in diatomic molecules. Phys Rev A: At Mol Opt Phys 2014;90:063427. doi:10.1103/PhysRevA.90.063427.
[6] Moses S, Covey J, Miecnikowski M, Jin D, Ye J. New frontiers for quantum gases of polar molecules. Nat Phys 2016;13:13–20. doi:10.1038/nphys3985.
[7] Keating T, Baldwin CH, Jau Y-Y, Lee J, Biedermann GW, Deutsch IH. Arbitrary Dicke-state control of symmetric Rydberg ensembles. Phys Rev Lett 2016;117:213601. doi:10.1103/PhysRevLett.117.213601.
[8] Andrè A, DeMille D, Doyle JM, Lukin MD, Maxwell SE, Rabl P, et al. A coherent all-electrical interface between polar molecules and mesoscopic superconducting resonators. Nat Phys 2006;2(9):636–42. doi:10.1038/nphys386.
[9] Ni K-K, Ospelkaus S, de Miranda MHG, Pe'er A, Neyenhuis B, Zirbel JJ, et al. A high phase-space-density gas of polar molecules. Science 2008;322(5899):231–5. doi:10.1126/science.1163861.
[10] Tada T. Hyperfine switching triggered by resonant tunneling for the detection of a single nuclear spin qubit. Phys Lett A 2008;372(44):6690–3. doi:10.1016/j.physleta.2008.09.020.
[11] Brown NC, Brown KR. Comparing Zeeman qubits to hyperfine qubits in the context of the surface code: $^{174}Yb^+$ and $^{171}Yb^+$. Phys Rev A: At Mol Opt Phys 2018;97:052301. doi:10.1103/PhysRevA.97.052301.
[12] Sikorsky T, Morita M, Meir Z, Buchachenko AA, Ben-shlomi R, Akerman N, et al. Phase locking between different partial waves in atom-ion spin-exchange collisions. Phys Rev Lett 2018;121:173402. doi:10.1103/PhysRevLett.121.173402.
[13] Ni K-K, Rosenband T, Grimes DD. Dipolar exchange quantum logic gate with polar molecules. Chem Sci 2018;9:6830–8. doi:10.1039/C8SC02355G.
[14] Han HS, Lee HG, Cho D. Site-specific and coherent manipulation of individual qubits in a 1D optical lattice with a 532-nm site separation. Phys Rev Lett 2019;122:133201. doi:10.1103/PhysRevLett.122.133201.

[15] Lang JE, Madhavan T, Tetienne J-P, Broadway DA, Hall LT, Teraji T, et al. Non-vanishing effect of detuning errors in dynamical-decoupling-based quantum sensing experiments. Phys Rev A: At Mol Opt Phys 2019;99:012110. doi:10.1103/PhysRevA.99.012110.

[16] Baranov MA, Dalmonte M, Pupillo G, Zoller P. Condensed matter theory of dipolar quantum gases. Chem Rev 2012;112(9):5012–61. doi:10.1021/cr2003568.

[17] DeMille D, Sainis S, Sage J, Bergeman T, Kotochigova S, Tiesinga E. Enhanced sensitivity to variation of $m_e/m_p$ in molecular spectra. Phys Rev Lett 2008;100(4):043202. doi:10.1103/PhysRevLett.100.043202.

[18] Beloy K, Borschevsky A, Flambaum VV, Schwerdtfeger P. Effect of $\alpha$ variation on a prospective experiment to detect variation of $m_e/m_p$ in diatomic molecules. Phys Rev A: At Mol Opt Phys 2011;84(4):042117. doi:10.1103/PhysRevA.84.042117.

[19] Sainis S, Sage J, Tiesinga E, Kotochigova S, Bergeman T, DeMille D. Detailed spectroscopy of the $Cs_2 a^3\Sigma_u^+$ state and implications for measurements sensitive to variation of the electron–proton mass ratio. Phys Rev A: At Mol Opt Phys 2012;86(2):022513. doi:10.1103/PhysRevA.86.022513.

[20] Safronova MS, Budker D, DeMille D, Kimball DFJ, Derevianko A, Clark CW. Search for new physics with atoms and molecules. Rev Mod Phys 2018;90:025008. doi:10.1103/RevModPhys.90.025008.

[21] Li D, Xie F, Li L, Magnier S, Sovkov VB, Ivanov VS. The $3^3\Sigma_g^+$ and $a^3\Sigma_u^+$ states of $Cs_2$: Observation and calculation. Chem Phys Lett 2007;441(1–3):39–42. doi:10.1016/j.cplett.2007.04.082.

[22] Xie F, Li D, Tyree L, Li L, Sovkov VB, Ivanov VS, et al. Observation and calculation of the $Cs_2 2^3\Delta_{1g}$ and $b^3\Pi_{0u}$ states. J Chem Phys 2008;128:204313. doi:10.1063/1.2920191.

[23] Xie F, Sovkov VB, Lyyra AM, Li D, Ingram S, Bai J, et al. Experimental investigation of the $Cs_2 a^3\Sigma_u^+$ triplet ground state: multiparameter Morse long range potential analysis and molecular constants. J Chem Phys 2009;130(5):051102. doi:10.1063/1.3075580.

[24] Xie F, Li L, Li D, Sovkov VB, Minaev KV, Ivanov VS, et al. Joint analysis of the $Cs_2 a^3\Sigma_u^+$ and $1_g$ ($3^3\Pi_{1g}$) states. J Chem Phys 2011;135(2):024303. doi:10.1063/1.3606397.

[25] Sovkov VB, Ivanov VS. Binding energies of the ground triplet state $a^3\Sigma_u^+$ of $Rb_2$ and $Cs_2$ in terms of the generalized Le Roy–Bernstein near–dissociation expansion. J Chem Phys 2014;140(13):134307. doi:10.1063/1.4869981.

[26] Ma J, Liu W, Yang J, Wu J, Sun W, Ivanov VS, et al. New observation and combined analysis of the $Cs_2 0_g^-$, $0_u^+$ and $1_g$ states at the asymptotes $6S_{1/2}+6P_{1/2}$ and $6S_{1/2}+6P_{3/2}$. J Chem Phys 2014;141(24):244310. doi:10.1063/1.4904265.

[27] Liu W, Xu R, Wu J, Yang J, Lukashov SS, Sovkov VB, et al. Observation and deperturbation of near–dissociation ro–vibrational structure of the $Cs_2$ state $0_u^+$ ($A^1\Sigma_u^+ \sim b^3\Pi_{0^+u}$) at the asymptote $6S_{1/2}+6P_{1/2}$. J Chem Phys 2015;143(12):124307. doi:10.1063/1.4931646.

[28] Sovkov VB, Xie F, Lyyra AM, Ahmed EH, Ma J, Jia S. Re-examination of the $Cs_2$ ground singlet $X^1\Sigma_g^+$ and triplet $a^3\Sigma_u^+$ states. J Chem Phys 2017;147(10):104301. doi:10.1063/1.5001481. See erratum in [29]

[29] Sovkov VB, Xie F, Lyyra AM, Ahmed EH, Ma J, Jia S. Erratum: Re-examination of the $Cs_2$ ground singlet $X^1\Sigma_g^+$ and triplet $a^3\Sigma_u^+$ states [J. Chem. Phys. **147**, 104301 (2017)]. J Chem Phys 2018;149(23):239901. doi:10.1063/1.5083024. Erratum to [28]

[30] Feng G, Li Y, Wang X, Wu J, Sovkov VB, Ma J, et al. Manipulation of photoassociation of ultracold Cs atoms with tunable scattering length by external magnetic fields. Sci Rep 2017;7(1):13677. doi:10.1038/s41598-017-13534-6.

[31] Li L, Zhu Q, Field RW. Hyperfine structure of the $Na_2 1^3\Delta_g$ state. J Mol Spectrosc 1989;134(1):50–62. doi:10.1016/0022-2852(89)90127-6.

[32] Liu Y, Ji B, Cheung AS-C, Stwalley WC, Field RW, Lyyra AM, et al. The hyperfine structure of the $1^3\Delta_g$ state of $Na_2$. J Chem Phys 2001;115(8):3647–56. doi:10.1063/1.1388548.

[33] Liu Y, Li L, Lazarov G, Lazoudis A, Lyyra AM, Field RW. Hyperfine structure of the $2^3\Sigma_g^+$, $3^3\Sigma_g^+$, and $4^3\Sigma_g^+$ states of $Na_2$. J Chem Phys 2004;121(12):5821–7. doi:10.1063/1.1780162.

[34] Xie F, Minaev KV, Sovkov VB, Ivanov VS, Li D, Li L. The hyperfine structure analysis of the $K_2 2^3\Sigma_g^+$ state. Chem Phys Lett 2010;493(4–6):238–41. doi:10.1016/j.cplett.2010.05.060.

[35] Minaev KV, Gruzdev MD, Ovchinnikova NE, Vaidner AO, Ivanov VS, Sovkov VB. Hyperfine structure in spectra of diatomic molecules: accurate and approximate computational schemes. Vestnik St Petersburg University Ser-4 2010;3:38–47. In Russian

[36] Takekoshi T, Strauss C, Lang F, Denschlag JH, Lysebo M, Veseth L. Hyperfine, rotational, and Zeeman structure of the lowest vibrational levels of the $^{87}Rb_2(1)^3\Sigma_g^+$ state. Phys Rev A: At Mol Opt Phys 2011;83(6):062504. doi:10.1103/PhysRevA.83.062504.

[37] Nayak MK, Chaudhuri RK. Determination of molecular hyperfine–structure constant using the second-order relativistic many–body perturbation theory. Phys Rev A: At Mol Opt Phys 2011;83(2):022504. doi:10.1103/PhysRevA.83.022504.

[38] Lysebo M, Veseth L. Molecular hyperfine parameters in the $1^3\Sigma_u^+$ and $1^3\Sigma_g^+$ states of $Li_2$, $Na_2$, $K_2$, and $Rb_2$. Eur Phys J D 2013;67(7):142. doi:10.1140/epjd/e2013-40062-1.

[39] Jelassi H, Pruvost L. Weakly bound $^{87}Rb_2(5s_{1/2}+5p_{1/2})1_g$ molecules: Hyperfine interaction and LeRoy-Bernstein analysis including linear and nonlinear terms. Phys Rev A: At Mol Opt Phys 2014;89(3):032514. doi:10.1103/PhysRevA.89.032514.

[40] Anderson DA, Miller SA, Raithel G. Angular-momentum couplings in long-range $Rb_2$ Rydberg molecules. Phys Rev A: At Mol Opt Phys 2014;90(6):062518. doi:10.1103/PhysRevA.90.062518.

[41] Orbán A, Vexiau R, Krieglsteiner O, Nägerl H-C, Dulieu O, Crubellier A, et al. Model for the hyperfine structure of electronically excited KCs molecules. Phys Rev A: At Mol Opt Phys 2015;92(3):032510. doi:10.1103/PhysRevA.92.032510.

[42] Deiss M, Drews B, Denschlag JH, Tiemann E. Mixing of $0^+$ and $0^-$ observed in the hyperfine and Zeeman structure of ultracold $Rb_2$, molecules. New J Phys 2015;17(Aug.):083032. doi:10.1088/1367-2630/17/8/083032.

[43] Böttcher F, Gaj A, Westphal KM, Schlagmüller M, Kleinbach KS, Löw R, et al. Observation of mixed singlet-triplet $Rb_2$ Rydberg molecules. Phys Rev A: At Mol Opt Phys 2016;93(3):032512. doi:10.1103/PhysRevA.93.032512.

[44] Sokolov IM. Influence of the hyperfine structure of the atomic states on the collective effects in the $Rb_2$ quasi-molecule. J Exp Theor Phys 2017;125(4):551–63. doi:10.1134/S1063776117090175. Translation of Zhurnal Experimentalnoi i Teoreticheskoi Physiki, vol. 125, No. 4, pp. 650–665 (2017)

[45] Orbán A, Xie T, Vexiau R, Dulieu O, Bouloufa-Maafa N. Hyperfine structure of electronically-excited states of the $^{39}K^{133}Cs$ molecule. J Phys B: At Mol Opt Phys 2019;52(13):135101. doi:10.1088/1361-6455/ab1d94.

[46] Quéméner G, Julienne PS. Ultracold molecules under control!. Chem Rev 2012;112(9):4949–5011. doi:10.1021/cr300092g.

[47] Guo M, Zhu B, Lu B, Ye X, Wang F, Vexiau R, et al. Creation of an ultracold gas of ground-state dipolar $^{23}Na^{87}Rb$ molecules. Phys Rev Lett 2016;116:205303. doi:10.1103/PhysRevLett.116.205303.

[48] Liu W, Wu J, Ma J, Li P, Sovkov VB, Xiao L, et al. Observation and analysis of the hyperfine structure of near-dissociation levels of the NaCs $c^3\Sigma^+$ state below the dissociation limit $3S_{1/2}+6P_{3/2}$. Phys Rev A: At Mol Opt Phys 2016;94(3):032518. doi:10.1103/PhysRevA.94.032518.

[49] Liu W, Wang X, Wu J, Su X, Wang S, Sovkov VB, et al. Experimental observation and determination of the laser-induced frequency shift of hyperfine levels of ultracold polar molecules. Phys Rev A: At Mol Opt Phys 2017;96(2):022504. doi:10.1103/PhysRevA.96.022504.

[50] Wu J, Liu W, Wang X, Ma J, Li D, Sovkov VB, et al. Observation of photoassociation of ultracold sodium and cesium at the asymptote Na ($3S_{1/2}$) + Cs ($6P_{1/2}$). J Chem Phys 2018;148(17):174304. doi:10.1063/1.5023330.

[51] Liu LR, Hood JD, Yu Y, Zhang JT, Hutzler NR, Rosenband T, et al. Building one molecule from a reservoir of two atoms. Science 2018;360(6391):900–3. doi:10.1126/science.aar7797.

[52] Feng G, Li Y, Wu J, Sovkov VB, Ma J, Xiao L, et al. Optical levitation-associated atomic loading in a dipole trap. Laser Phys 2019;29(3):035505. doi:10.1088/1555-6611/aafd22.

[53] De Marco L, Valtolina G, Matsuda K, Tobias WG, Covey JP, Ye J. A degenerate Fermi gas of polar molecules. Science 2019;363(6429):853–6. doi:10.1126/science.aau7230.

[54] Wang X, Liu W, Wu J, Sovkov VB, Ma J, Li P, et al. Saturation of photoassociation in NaCs dark magneto-optical trap. J Quant Spectrosc Radiat Transfer 2020;240:106678. doi:10.1016/j.jqsrt.2019.106678.

[55] Li D, Xie F, Li L. Observation of the $Cs_2 3^3\Sigma_g^+$ state by infrared–infrared double resonance. Chem Phys Lett 2008;458(4–6):267–71. doi:10.1016/j.cplett.2008.04.115.

[56] Wang X, Liu W, Li Y, Wu J, Sovkov VB, Ma J, et al. Hyperfine structure of the NaCs $b^3\Pi_2$ state near the dissociation limit $3S_{1/2}+6P_{3/2}$ observed with ultracold atomic photoassociation. Phys Chem Chem Phys 2020;22(7):3809–16. doi:10.1039/C9CP05870B.

[57] Sovkov VB, Xie F, Li D, Lukashov SS, Baturo VV, Ma J, et al. Renewed analysis of the hyperfine structure of the $Na_2 1^3\Delta_g$ state. AIP Adv 2018;8(12):125322. doi:10.1063/1.5055675.

[58] Li L, Field RW. Direct observation of high–lying $^3\Pi_g$ states of the $Na_2$ molecule by optical–optical double resonance. J Phys Chem 1983;87(16):3020–2. doi:10.1021/j100239a011.

[59] Li L, Rice SF, Field RW. The $Na_2 a^3\Sigma_u^+$ state. Rotationally resolved OODR $^3\Pi_g \rightarrow a^3\Sigma_u^+$ fluorescence spectroscopy. J Chem Phys 1985;82(3):1178–82. doi:10.1063/1.448490.

[60] Whang T-J, Tsai C-C, Stwalley WC, Lyyra AM, Li L. Spectroscopic study of the $Na_2 2^3\Sigma_g^+$ state by cw perturbation–facilitated optical–optical double–resonance spectroscopy. J Mol Spectrosc 1993;160(2):411–21. doi:10.1006/jmsp.1993.1188.

[61] Li L, Li M. Deperturbation of the $Na_2 4^3\Sigma_g^+ v=4 \sim 3^3\Pi_g v=6$ and $4^3\Sigma_g^+ v=14 \sim 2^3\Pi_g v=68$ interactions. J Mol Spectrosc 1995;173(1):25–36. doi:10.1006/jmsp.1995.1214.

[62] Ivanov VS, Sovkov VB. An IPA procedure for bound–continuum diatomic transition intensities. Chem Phys 1996;213(1–3):295–301. doi:10.1016/S0301-0104(96)00304-7.

[63] Li L, Lyyra AM. Triplet states of $Li_2$ and $Na_2$: Perturbation facilitated optical–optical double resonance spectroscopy. Spectrochimica Acta Part A 1999;55(11):2147–78. doi:10.1016/S1386-1425(99)00091-8.

[64] Ivanov VS, Sovkov VB. Inversion procedures for bound–free diatomic transition intensities. Application to the PFOODR spectra of $^7Li_2$. Proceedings of SPIE 1997;3090:150–6. doi:10.1117/12.267754.

[65] Li J, Liu Y, Chen H, Xiang J, Chen D, Wu G, et al. Predissociation of the $Na_2 4^3\Sigma_g^+$ state. J Chem Phys 1998;108(18):7707–12. doi:10.1063/1.476206.

[66] Ivanov VS, Sovkov VB, Serov VN, Li L. Inversion procedures for the PFOODR experimental data on the $Li_2$ molecule. Proceedings of SPIE 1999;3732:187–94. doi:10.1117/12.340010.

[67] Ivanov VS, Sovkov VB, Li L, Lyyra AM, Whang T-J, Magnier S. Analysis of the $Na_2\,2^3\Sigma_g^+ \longrightarrow a^3\Sigma_u^+$ continua: Potentials and transition moment function. J Chem Phys 2001;114(14):6077–85. doi:10.1063/1.1355979.

[68] Ivanov VS, Sovkov VB, Gallice N, Li L, Liu Y, Lyyra AM, et al. Use of bound–free structured spectra in determining RKR potentials: The $4^3\Pi_g$ state of $Na_2$. J Mol Spectrosc 2001;209(1):116–21. doi:10.1006/jmsp.2001.8413.

[69] Yi P, Dai X, Li J, Liu Y, Li L, Sovkov VB, et al. The $6^3\Sigma_g^+$ state of $Na_2$: Observations and analysis. J Mol Spectrosc 2004;225(1):33–8. doi:10.1016/j.jms.2004.02.005.

[70] Chu Y, Xie F, Li D, Li L, Sovkov VB, Ivanov VS, et al. Experimental study of the $^{39}K_2\,2^3\Pi_g$ state by perturbation facilitated infrared–infrared double resonance and two–photon excitation spectroscopy. J Chem Phys 2005;122(7):074302. doi:10.1063/1.1843815.

[71] Ahmed E, Lyyra AM, Li L, Ivanov VS, Sovkov VB, Magnier S. Revision of the $K_2\,3^3\Pi_g$ and $4^3\Sigma_g^+$ states: new vibrational numberings and new potential functions. J Mol Spectrosc 2005;229(1):122–30. doi:10.1016/j.jms.2004.08.021.

[72] Xie F, Li D, Li L. Experimental observation of the triplet states of $^{39}K_2$ by infrared-infrared double resonance spectroscopy. The 2nd international conference on modern trends in physics research (MTPR-06). AIP Conf Proc 2007;888(1):3–7. doi:10.1063/1.2711083.

[73] Xie F, Li D, Li L, Field RW, Magnier S. Infrared–infrared double resonance spectroscopy of $^{39}K_2$: The $1^3\Delta_g$ state. Chem Phys Lett 2006;431(4):267–71. doi:10.1016/j.cplett.2006.10.002.

[74] Xie F, Li D, Chu Y, Li L, Magnier S, Sovkov VB, et al. The $K_2\,2^3\Pi_g$ state: new observations and analysis. J Phys Chem A 2006;110(39):11260–4. doi:10.1021/jp063266m.

[75] Li D, Xie F, Li L, Sovkov VB, Ivanov VS, Ahmed E, et al. The $^{39}K_2\,2^3\Sigma_g^+$ state: observation and analysis. J Chem Phys 2007;126(19):194314. doi:10.1063/1.2730804.

[76] Sovkov VB, Ivanov VS, Li D, Xie F, Li L. Combined analysis of the PFOODR data on the $a^3\Sigma_u^+$, $2^3\Pi_g$, $2^3\Sigma_g^+$, $3^3\Pi_g$, and $4^3\Sigma_g^+$ states of the $K_2$ molecule. Optics & Spectroscopy 2007;103(5):723–7. doi:10.1134/S0030400X07110069. Translated from Optika i Spektroskopiya, 2007, Vol. 103, No. 5, pp. 747–751

[77] Guan Y, Han X, Yang J, Zhou Z, Dai X, Ahmed EH, et al. Updated potential energy function of the $Rb_2\,a^3\Sigma_u^+$ state in the attractive and repulsive regions determined from its joint analysis with the $2^3\Pi_{0g}$ state. J Chem Phys 2013;139(14):144303. doi:10.1063/1.4823496.

[78] Li D, Xie F, Li L, Ahmed EH, Lyyra AM. Collisional line assignments and hyperfine structure interpretation in $Cs_2\,2^3\Delta_{1g}$ state. Chin J Chem Phys 2013;26(1):13–19. doi:10.1063/1674-0068/26/01/13-19.

[79] Sovkov VB, Ivanov VS. WKB–kind integrals in the generalized Le Roy–Bernstein theory of diatomic near–dissociation levels. Vestnik St Petersburg Univ Ser-4 2014;1(59)(4):473–8.

[80] Yang J, Guan Y, Zhao W, Zhou Z, Han X, Ma J, et al. Observations and analysis with the spline–based Rydberg–Klein–Rees approach for the $3^1\Sigma_g^+$ state of $Rb_2$. J Chem Phys 2016;144(2):024308. doi:10.1063/1.4939524.

[81] Arndt PT, Sovkov VB, Ma J, Pan X, Beecher DS, Tsai JY, et al. The $Rb_2\,3^1\Pi_g$ state: Observation and analysis. J Chem Phys 2018;149(22):224303. doi:10.1063/1.5058282.

[82] Arndt PT, Sovkov VB, Ma J, Pan X, Beecher DS, Tsai JY, et al. Experimental study of the $6^1\Sigma_g^+$ state of the rubidium dimer. Phys Rev A: At Mol Opt Phys 2019;99(5):052511. doi:10.1103/PhysRevA.99.052511.

[83] Li L, Lazoudis A, Yi P, Liu Y, Huennekens J, Field RW, et al. Hyperfine structure of the $1^3\Delta_g$, $2^3\Pi_g$, and $3^3\Sigma_g^+$ states of $^6Li^7Li$. J Chem Phys 2002;116(24):10704–12. doi:10.1063/1.1478692.

[84] Burns P, Sibbach-Morgus L, Wilkins AD, Halpern F, Clarke L, Miles RD, et al. The $4^3\Sigma^+$ state of NaK: potential energy curve and hyperfine structure. J Chem Phys 2003;119(9):4743–54. doi:10.1063/1.1590638.

[85] Wilkins AD, Morgus L, Hernandez-Guzman J, Huennekens J, Hickman AP. The NaK $1^{1,3}\Delta$ states: theoretical and experimental studies of fine and hyperfine structure of rovibrational levels near the dissociation limit. J Chem Phys 2005;123(12):124306. doi:10.1063/1.2010471.

[86] Burns P, Wilkins AD, Hickman AP, Huennekens J. The NaK $1(b)^3\Pi_{\Omega=0}$ state hyperfine structure and the $1(b)^3\Pi_{\Omega=0} \sim 2(A)^1\Sigma^+$ spin–orbit interaction. J Chem Phys 2005;122(7):074306. doi:10.1063/1.1844293.

[87] Zare RN. Angular momentum: understanding spatial aspects in chemistry and physics. New York–Chichester–Brisbane–Toronto–Sigapore: John Wiley & Sons; 1988.

[88] Lefebvre-Brion H, Field RW. The spectra and dynamics of diatomic molecules. Amsterdam–Boston–Heidelberg–New York–Oxford-Paris–San Diego–San Francisco–Singapore–Sydney–Tokio: Elsevier. Academic Press; 2004.

[89] Li D. Laser spectroscopic studies on the triplet states of $Cs_2$ and $Li_2$ molecules, Ph.D. thesis. Tsinghua University; 2008. In Chinese

[90] Pupyshev VI, Pazyuk EA, Stolyarov AV, Tamanis M, Ferber R. Analogue of oscillation theorem for nonadiabatic diatomic states: application to the $A^1\Sigma^+$ and $b^3\Pi$ states of KCs. Phys Chem Chem Phys 2010;12(18):4809–12. doi:10.1039/B918384A.

[91] Bai J, Ahmed EH, Beser B, Guan Y, Kotochigova S, Lyyra AM, et al. Global analysis of data on the spin–orbit–coupled $A^1\Sigma_u^+$ and $b^3\Pi_u$ states of $Cs_2$. Phys Rev A: At Mol Opt Phys 2011;83(3):032514. doi:10.1103/PhysRevA.83.032514.

[92] Znotins A, Kruzins A, Tamanis M, Ferber R, Pazyuk EA, Stolyarov AV, et al. Fourier-transform spectroscopy, relativistic electronic structure calculation, and coupled-channel deperturbation analysis of the fully mixed $A^1\Sigma_u^+$ and $b^3\Pi_u$ states of $Cs_2$. Phys Rev A: At Mol Opt Phys 2019;100(4):042507. doi:10.1103/PhysRevA.100.042507.

[93] Qi P, Bai J, Ahmed E, Lyyra AM, Kotochigova S, Ross AJ, et al. New spectroscopic data, spin–orbit functions, and global analysis of data on the $A^1\Sigma_u^+$ and $b^3\Pi_u$ states of $na_2$. J Chem Phys 2007;127(4):044301. doi:10.1063/1.2747595.

[94] Martson CC, Balint-Kurti GG. The Fourier grid Hamiltonian method for bound state eigenvalues and eigenfunctions. J Chem Phys 1989;91(6):3571–6. doi:10.1063/1.456888.

[95] Dulieu O, Julienne PS. Coupled channel bound states calculations for alkali dimers using the Fourier grid method. J Chem Phys 1995;103(1):60–6. doi:10.1063/1.469622.

[96] Willner K, Dulieu O, Masnou-Seeuws F. Mapped grid methods for long-range molecules and cold collisions. J Chem Phys 2004;120(2):548–61. doi:10.1063/1.1630031.

[97] Sovkov VB, Ma J. Matlab tool “Optimizer”: Construction and optimization of multi-block mathematical models—application to spectroscopy experiments with ultracold gases of alkali metals. In: Dadvand A, Nagaraja K, Mirzazadeh M, editors. Proceedings of the 2016 international conference on applied mathematics, simulation and modelling, Advances in Computer Science Research. Beijing, China: Atlantis Press; 2016. p. 369–372(No. 083). doi:10.2991/amsm-16.2016.83.

[98] Sovkov VB. Optimizer: source codes and manuals; 2019. Online; https://sourceforge.net/projects/optimizer-sovkov/.